THE JOURNAL OF BIOLOGICAL CHEMISTRY VOL. 288, NO. 39, pp. 28089–28103, September 27, 2013

The Interaction Surface of a Bacterial Transcription Elongation Factor Required for Complex Formation with an Antiterminator during Transcription Antitermination*

Received for publication, March 25, 2013, and in revised form, August 2, 2013 Published, JBC Papers in Press, August 2, 2013, DOI 10.1074/jbc.M113.472209

Saurabh Mishra[1], **Shalini Mohan, Sapna Godavarthi, and Ranjan Sen**[2]

From the Laboratory of Transcription, Centre for DNA Fingerprinting and Diagnostics, Tuljaguda Complex, 4-1-714 Mozamjahi Road, Nampally, Hyderabad-500001, India

Background: The mode of interaction between the transcription factor, NusA, and the antiterminator, N, is unknown.
Results: When bound to the transcription elongation complex (EC), NusA-NTD interacts with N.
Conclusion: The EC-induced away-movement of NusA-C-terminal domain changed the interaction surface of NusA for N.
Significance: N-NusA interaction converts NusA into an antiterminator by influencing the NusA-RNA polymerase interaction.

The bacterial transcription elongation factor, NusA, functions as an antiterminator when it is bound to the lambdoid phage derived antiterminator protein, N. The mode of N-NusA interaction is unknown, knowledge of which is essential to understand the antitermination process. It was reported earlier that in the absence of the transcription elongation complex (EC), N interacts with the C-terminal AR1 domain of NusA. However, the functional significance of this interaction is obscure. Here we identified mutations in NusA N terminus (NTD) specifically defective for N-mediated antitermination. These are located at a convex surface of the NusA-NTD, situated opposite its concave RNA polymerase (RNAP) binding surface. These NusA mutants disrupt the N-*nut* site interactions on the nascent RNA emerging out of a stalled EC. In the N/NusA-modified EC, a Cys-53 (S53C) from the convex surface of the NusA-NTD forms a specific disulfide (S-S) bridge with a Cys-39 (S39C) of the NusA binding region of the N protein. We conclude that when bound to the EC, the N interaction surface of NusA shifts from the AR1 domain to its NTD domain. This occurred due to a massive away-movement of the adjacent AR2 domain of NusA upon binding to the EC. We propose that the close proximity of this altered N-interaction site of NusA to its RNAP binding surface, enables N to influence the NusA-RNAP interaction during transcription antitermination that in turn facilitates the conversion of NusA into an antiterminator.

Escherichia coli RNAP terminates transcription at the intrinsic terminators composed of specific RNA sequences or when it is dislodged by the nascent RNA-binding protein, Rho (1, 2). Lambdoid phages encode proteins, like N and Q, that make the EC[3] termination resistant. This phenomenon is called transcription antitermination (Refs. 3 and 4; Fig. 1*A*).

The antiterminator, N, is a small basic protein that binds to a specific stem-loop structure (*box B* of *nut* site; Fig. 1*B*) of the mRNA through its N-terminal arginine rich motif (ARM; Refs. 5 and 6; Fig. 1, *C* and *D*) and interacts with the RNAP through its C terminus (7, 8). N requires several host-factors, called Nus factors, for processive antitermination (Ref. 4 and Fig. 1*C*). N and these Nus factors assemble on the *nut* (N utilization) site of the mRNA, where N and NusA make specific interactions (Ref. 3 and Fig. 1*C*).

The elongation/termination factor NusA is a ~55-kDa protein having the following functional domains: an N-terminal RNAP binding domain (NTD), three RNA binding domains (S1, KH1, and KH2), and two C-terminal acidic repeats (AR1 and AR2) (Ref. 9 and Fig. 1*E*). A concave surface of the NusA-NTD interacts with the flap domain of the β-subunit of RNAP (10, 11), whereas the AR2 domain binds to the C-terminal domain (α-CTD) of the α-subunit of RNAP (12). NusA enhances intrinsic termination (13, 14), induces transcription pausing (15–17), and functions as an antiterminator upon forming a complex with the N protein (14).

The N-NusA interaction at the *nut* site is essential to convert the latter into an antiterminator. In the absence of the EC, the AR1 region of NusA specifically interacts with the N protein (Ref. 18 and Fig. 1*F*). However, the functional relevance of NusA AR1-N interaction is obscure (18). Understanding the mode of interaction of NusA with N as well as with RNAP during the process of transcription elongation is essential to know the mechanism of antitermination.

Here, we show that NusA AR1-N interaction is not important both in the *in vivo* and *in vitro* antitermination assays, and this interaction is also not required for the bacteriophage growth. We have identified point mutations at a convex surface located opposite the RNAP binding surface of the NusA-NTD that are specifically defective for N-mediated transcription antitermination. These mutants affected the binding of N-NusA complex to the *nut* site, present on the mRNA emerging out of a stalled EC. In this same EC, the Ser-53 of the NusA-NTD that was replaced with a Cys specifically formed a S-S bridge with another Cys, Cys-39 (replacing the native Ser-39), from the NusA binding region of

* This work was supported by the Department of Science and Technology, Government of India and Centre for DNA Fingerprinting and Diagnostics intramural funding.
[1] A Senior Research Fellow of Indian Council of Medical Research, toward a Ph.D. from the Manipal University.
[2] A Swarnajayanti fellow of the Department of Science and Technology. To whom correspondence should be addressed. Tel.: 91-40-24749428; Fax: 91-40-24749343; E-mail: rsen@cdfd.org.in.
[3] The abbreviations used are: EC, elongation complex; RNAP, RNA polymerase; NTD, N-terminal domain; Ni-NTA, nickel-nitrilotriacetic acid; RT, read-through; RB, road-blocked; oligo, oligonucleotide; %RT, terminator read-through efficiency.

the N protein. We concluded that upon binding to the EC, the interaction surface of NusA for N changes from the NusA-AR1 region to its NTD domain. Most likely this occurs due to the away-movement of the AR2 domain of NusA upon binding to the EC. We propose that the close proximity of this altered N-interaction site of NusA to its RNAP binding surface enables N to modulate the NusA-RNAP interaction during the antitermination process.

EXPERIMENTAL PROCEDURES

Materials—NTPs were purchased from GE Healthcare. [γ-^{32}P]ATP (3000 Ci/mmol) and [α-^{32}P]CTP (3000 Ci/mmol) were from Jonaki, BRIT, India. Antibiotics, isopropyl 1-thio-β-D-galactopyranoside, lysozyme, DTT, and BSA were from U. S. Biochemical Corp. Primers for PCR were obtained either from Sigma or MWG. Restriction endonucleases, polynucleotide kinase, and T4 DNA ligase were from New England Biolabs. WT *E. coli* RNAP holoenzyme was purchased from Epicenter Biotechnologies. TaqDNA polymerase was from Roche Applied Science. Ni-NTA-agarose beads were from Qiagen. Streptavidin-coated magnetic beads were from Promega. HPLC pure antisense oligos used in the footprinting experiments were from MWG. RNase T1 was from Ambion and RNase H was from Epicenter. All the bacterial growth media were from Difco.

Bacterial Strains, Plasmids, and Phages—All the bacterial strains, plasmids, and phages used are listed in Table 1. All the *in vivo* antitermination assays were performed in different derivatives of *E. coli* MC4100*rac*$^-$ strains. The strains RS1017, RS1148, RS734, RS445, RS1237, RS1245, and RS1019 used in β-galactosidase assays contain single-copy P_{lac}-H-19B *nutR/*t_{R1}*-trpt′-lacZYA*, P_{lac}-H-19B *nutR/*t_{R1}-$T_{R'}$-T1T2-*lacZYA*, P_{lac}-H-19B *nutR/*t_{R1}*-lacZYA*, P_{lac}*-lacZYA*, P_{lac}-λ *nutR/*t_{R1}-$T_{R'}$-T1T2-*lacZYA*, P_{lac}-λ *nutR/*t_{R1}*-trpt′-lacZYA*, and P_{lac}-λ *nutR/*t_{R1}*-lacZYA* reporter cassettes, respectively, as λRS45 lysogens. t_{R1} and *trpt′* are Rho-dependent, and $T_{R'}$, T1, and T2 are the Rho-independent terminators. In all these reporters, expression of *lacZ* occurs only in the presence of the N-mediated antitermination. In the construct *nutR/*t_{R1}*-trpt*, t_{R1} and *trpt′* are fused in tandem (19).

Random Mutagenesis and Screening of NusA Mutants—The plasmid pRS703, containing *nusA*, was transformed into a XL1-Red mutator strain and was randomly mutagenized during its growth (20). The mutagenized plasmid library thus obtained was electroporated into the strain RS1017 (having the P_{lac}–*nutR/*t_{R1}*-trpt′-lacZYA* reporter as a lysogen) containing the pK8601 plasmid with the *N* gene from the lambdoid phage H-19B. The transformants were plated on LB media supplemented with appropriate antibiotics, and the survivors were scraped and inoculated in 10 ml of LB and incubated for 30 min. This culture was made *nusA* null (*nusA*::*cam*^{R}; Ref. 21) by P1 transduction, and the transductants were plated on MacConkey-lactose plates and screened for white colonies. NusA mutants defective for N-mediated antitermination appeared as white/pink colonies on these plates. Approximately 100,000 colonies were screened. The mutations were confirmed by sequencing. It should be noted that the *nusA*::*cam*^{R} (21) is not a complete deletion of *nusA*. A fragment containing NusA-NTD is produced in this strain. However, this fragment alone neither supports growth (data not shown) nor the N-mediated antitermination (data not shown). Therefore, in all our *in vivo* assays, we do not expect any interference from this NusA-NTD fragment.

Preparation of Other NusA Mutants—NusA mutants A11D, V8E, L31E, L27E, A7D, and V12D were made by site-directed mutagenesis. Deletion derivatives of NusA were made by overlapping-PCR methods and cloned in the plasmid pHyd3011 between the NdeI and SalI sites.

In Vivo Antitermination Assays—To measure the antitermination defects of the NusA C-terminal deletion derivatives, the plasmids (pHYD3011) containing WT *nusA* and the deletion derivatives, ΔAR2 (NusA:1–416) and ΔAR1-2 (NusA: 1–348), were transformed into the strains RS1017 (having P_{lac}-H-19B *nutR/*t_{R1}*-trpt′-lacZYA* construct as a lysogen) and RS445 (having P_{lac}*-lacZYA* construct as a lysogen), respectively, after which the chromosomal *nusA* was deleted by P1 transduction. The resultant strains were transformed with pK8601 having the H-19B or λ N genes. Similarly, strains RS1148 (with the reporter P_{lac}-H-19B *nutR-*$T_{R'}$*-T1-T2-lacZYA*) and RS734 (with the reporter P_{lac}-H-19B *nutR-lacZYA*) were also transformed with the above plasmids. β-Galactosidase activities were measured in a microtiter plate using a Spectramax plus plate reader by following the published procedures (22). The $T_{R'}$*-T1-T2-lacZYA* cassette measures the antitermination through the Rho-independent terminators, whereas the *nutR/*t_{R1}*-trpt′-lacZYA* measures the antitermination through the Rho-dependent terminators. The *in vivo* antitermination efficiency of the NusA deletion derivatives was expressed as the terminator read-through efficiency (%RT). The %RTs at different terminators were calculated using the following formula: [(β-galactosidase activities in the presence of terminators)/([(β-galactosidase activities in the absence of terminators)] × 100. To analyze the antitermination defects of the NusA point mutants, β-galactosidase activities were measured in the strains RS1017 and RS1148 in the presence and the absence of the H-19B N plasmid, pK8601. The same assays were performed with λ N plasmid, pRS256, using the strains, RS1245 (P_{lac}-λ *nutR/*t_{R1}*-trpt′-lacZYA* construct), RS1237 (P_{lac}-λ *nutR/*t_{R1}*- T1-T2-lacZYA* construct), RS1019 (P_{lac}-λ *nutR/*t_{R1}*-lacZYA* construct), and RS445. In Fig. 3 we have measured the antitermination efficiency by comparing the β-galactosidase activities obtained in the presence and absence of the N proteins.

Phage Spotting Assays—To check whether the mutant NusA proteins support the growth of phages H-19B and λ, plasmid containing WT and different NusA derivatives were transformed into the strain RS862, and chromosomal *nusA* was deleted. Serial dilutions of the bacteriophages H-19B (a gift from Dr. David Friedman) and λC1857 were spotted onto the lawns of RS862 (Fig. 2*C*). In some experiments plaques were also counted/scanned after overnight incubation at 37 °C (Fig. 3*F*).

Templates for in Vitro Transcriptions—Linear DNA templates for *in vitro* transcription assays were made by PCR amplification from the plasmids, pRS22 (T7A1-H-19B *nutR/*t_{R1}), pRS1092 (T7A1-H-19B *nutR/*t_{R1}*-trpt′*), pRS385 (pT7A1-H-19B *nutR/*t_{R1}*-lacO-tR′*), and pRS604 (pT7A1-λ *nutR/*t_{R1} -$T_{R'}$T1T2). When required, a *lac* operator sequence was inserted either after t_{R1} or *trpt′* terminator using a downstream primer having

TABLE 1
Strains, plasmids, phages, and oligos

	Description	Reference
Strains		
RS734	MC4100 *galEp3*, P_{lac}–H-19B *nutR*/t_{R1}-*lacZYA*	J. Gowrishankar
RS445	GJ3161, λRS88 lysogen carrying P_{lac}–*lacZYA*	22
RS862	MG1655 Δ*rac*::*tet*^{R}	J.Gowrishankar
RS1017	MC4100 *galEp3*, λRS45 lysogen carrying P_{lac}–H-19B *nutR*/t_{R1}- *trpt'-lacZYA*	This study
RS1019	MC4100 *galEp3*, P_{lac}–λ *nutR*-t_{R1}-*lacZYA*	This study
RS1148	MC4100 *galEp3*, λRS45 lysogen carrying P_{lac}–H-19B *nutR*/t_{R1}- $T_{R'}$-T1-T2–*lacZYA*	This study
RS1237	MC4100 *galEp3*, P_{lac}–λ *nutR*/t_{R1}-$T_{R'}$-*T1-T2- lacZYA*	This study
RS1245	MC4100 *galEp3*, λRS45 lysogen carrying P_{lac}–λ *nutR*/t_{R1}-*trpt'-lacZYA*	This study
XL1-Red	*endA1 gyrA96 thi-1 hsdR17 supE44 relA1 lac mutD5 mutS mutT* Tn*10* (*tet*^{R})	Stratagene
Phages		
λRS45, λ*cI857*		J. Gowrishankar
H-19B		David Friedman
Plasmids		
pK8601	pGB2 with P_{lac}-H-19B *N*, *spec*^{R}	38
pK8641	pTL61T with P_{lac}–H-19B-*nutR*-$T_{R'}$-T1-T2-*lacZYA* fusion. $T_{R'}$-T1-T2 is a triple terminator cassette, *amp*^{R}	38
pHYD3011	*nusA* and mutants of *nusA* were cloned into NdeI-SalI sites under pBAD promoter, *amp*^{R}	22
pRS12	H-19B *N* cloned at NdeI/XhoI site of pET21b, *amp*^{R}	23
pRS22	pTL61T with pT7A1–H-19B *nutR*-$T_{R'}$-T1-T2-*lac*ZYA, *amp*^{R}	23
pRS24	WT *nusA* cloned at NdeI/XhoI site of pET28b, His tag at N terminus, *kan*^{R}	23
pRS25	pTL61T with pT7A1–H-19B *nutR* (Δ*cII*) $T_{R'}$-T1-T2-*lacZYA*,*amp*^{R}	23
pRS256	pGB2 with P_{lac}-λ*N*, *spec*^{R}	19
pRS385	pRS25 with T7A1-*nutR-lac*O-$T_{R'}$ fusion, *amp*^{R}	33
pRS523	WT *nusA* cloned at NdeI/XhoI site of pET33b, HMK, His tag at N terminus, *kan*^{R}	33
pRS604	pTL61T with pT7A1–λ *nutR*-T1T2-*lac*ZYA, *amp*^{R}	
pRS615	λ*N* cloned at NdeI/XhoI site of pET21b, *amp*^{R}	
pRS703	pHyd3011 having WT *nusA*	This study
pRS1005	ΔAR1–2 NusA fragment cloned at NdeI/XhoI site of pET28b, His tag at N terminus, *kan*^{R}	This study
pRS1011	ΔAR2 NusA fragment cloned at NdeI/XhoI site of pET28b, His tag at N terminus, *kan*^{R}	This study
pRS1100	Zero-Cys *nusA* made by SDM on pET33b, HMK, his tag at N terminus, *kan*^{R}	This study
pRS1101	pHyd3011 having *nusA* V8A mutation	This study
pRS1102	C454S(C251, C489) *nusA* made by SDM on pET33b, HMK, his tag at N terminus, *kan*^{R}	This study
pRS1124	*nusA* S29C made by SDM on pRS1100, HMK, his tag at N-terminus, *kan*^{R}	This study
pRS1127	*nusA* V8A mutant cloned at NdeI/XhoI site of pET28b, His tag at N terminus, *kan*^{R}	This study
pRS1139	Phyd3011 having *nusA* V12D	This study
pRS1140	Phyd3011 having *nusA* V8E	This study
pRS1141	Phyd3011 having *nusA* L31E	This study
pRS1149	*nusA* V8E mutant cloned at NdeI/XhoI site of pET28b, His tag at N terminus, *kan*^{R}	This study
pRS1154	Phyd3011 having *nusA* A11D	This study
pRS1163	Phyd3011 having *nusA* A7D	This study
pRS1182	*nusA* V12D mutant cloned at NdeI/XhoI site of pET28b, His tag at N terminus, *kan*^{R}	This study
pRS1193	*nusA* S53C made by SDM on pRS1100, HMK, his tag at N-terminus, *kan*^{R}	This study
pRS1205	ΔAR1–2 NusA S53C cloned at NdeI/XhoI site of pET33b, HMK, his tag at N-terminus, *kan*^{R}	This study
pRS1313	*nusA* V8E S53C made by SDM on pRS1193, HMK, his tag at N-terminus, *kan*^{R}	This study
pRS1407	*nusA* T371C made by SDM on pRS1100, HMK, his tag at N-terminus, *kan*^{R}	This study
pRS1421	λ*N* C93S made by SDM on pRS615	This study
pRS1422	λ*N* S39C made by SDM on pRS1421	This study
pRS1425	39-Cys λ*N* sub-cloned in pET33b, HMK, his tag at N terminus, *kan*^{R}	This study
Oligos		
RK1	RS58 CGCCAGGGTTTTCCCAGTCACGAC; Reverse primer in the *lacZ* gene of pTL61T	
RS2	CTTGCATGCCTGCAGGTCGACTC; Reverse primer after $T_{R'}$ of pTL61T	
RK23b	TGGAGTTCCAGACGATACGTCG; reverse primer to generate T7A1- H-19B-*nutR*/t_{R1} terminator template	
RS58	ATAAACTGCCAGGAATTGGGGATCG; forward primer of pTL61T (and all its derivatives like pRS106, pRS25) vector sequence	
RS83	Biotinylated RS58	
RS147	GCGCGCGGATCCCCCCATTCAAGAACAGCAAGCAGC; reverse oligo to generate T7A1-λt_{R1} terminator template	
RS177	GAATTGTGAGCGCTCACAATTCggatATATATTAACAATTACCTG; lacO fusion at 161U of trpt′ terminator	
RS367	5′ GGA ATG TGT AAG AGC GGG GTT ATT TAT GC 3′ 29-mer, antisense oligo to λ rutA, boxA, and spacer RNA	
RS663	CGTAGGACGAATGTCCATTGTG; antisense to *nutR spacer* of H-19B	

the operator sequence. In pRS385, the *lac* operator sequence is cloned after the t_{R1} terminator (23). 5′-Biotinylation of the templates was incorporated by using the biotinylated primer RS83, and the immobilization was done on streptavidin-coated magnetic beads (Promega). In all the templates transcription was initiated from the T7A1 promoter.

In Vitro Transcription Assays—For the transcription on the T7A1-*nutR*-$T_{R'}$-*T1-T2* and T7A1-*nutR*-$T_{R'}$ templates (Figs. 2*B*, 4*C*, and 7*C*), reactions were carried out in T-Glu buffer (20 mM Tris-glutamate, pH 8.0, 10 mM magnesium glutamate, 50 mM potassium glutamate, 1 mM DTT, and 100 μg/ml BSA) at 32 °C. The reactions were initiated with 175 μM ApU, 5 μM GTP, 5 μM ATP, 2.5 μM CTP, and [α-^{32}P]CTP (3000Ci/mmol) to make a 23-mer EC (EC_{23}). Then it was chased with 250 μM each of all the NTPs in the presence of 300 nM of WT and mutant NusA proteins, 100 nM H19B or λN and 200 nM NusG. The reactions were stopped by extraction with phenol followed by ethanol precipitation. Samples were loaded onto a 6% sequencing gel and analyzed using FLA 9000 phosphorimaging (Fuji). For the transcription reactions on the T7A1-H-19B *nutR*/t_{R1}-*trpt'* and T7A1-λ*nutR*/t_{R1} template, reactions were carried out in T-Cl buffer (25 mM Tris-Cl (pH 8.0), 10 mM $MgCl_2$, and 50 mM KCl) at 37 °C. Other reaction conditions remained the same. For Rho-independent terminators the %

read-through (%RT) values were obtained by: %RT = [(RO)/(RO) + $T_{R'}$ + T1 + T2]. For Rho-dependent terminators, it was calculated as %RT = [RO/RO + (total products in the terminator zone)].

RNase H and RNase T1 Footprinting—For the footprinting experiments with H-19B N protein, a stalled EC (RB; road-blocked) was formed at the *lac* operator site of the template, T7A1-H-19B *nutR-lacO*. For λ N, the RB was formed on T7A1-λ *nutR*-lacO template (amplified from pRS604; data not shown). RB was formed by transcribing this template in a similar way as described above, with 50 nM RNAP and 10 nM immobilized biotinylated DNA templates on streptavidin-coated magnetic beads, except that 100 nM lac repressor was present in this case. The EC_{23} was chased to the lac operator site by transcribing with 250 μM NTPs. The RB was incubated for 5 min with 150 nM concentrations of either WT or mutant NusA and 150 nM of H-19B N or λ N. The RB, attached to the streptavidin beads, was then extensively washed to remove free proteins (RNAP, NusA, N etc.). However, we observed the presence of inactivated EC_{23} complexes (un-chased) even after chasing with all the NTPs. These complexes could not be removed upon washing. EC_{23} contains a very short RNA, which is not expected to interfere with the footprinting of the longer RNA associated with the RB complexes. Hence, our RB preparations did not have any free proteins but presumably would contain inactive EC_{23} complexes, and the amount of this complex varied between different experiments. We used about a 10-fold molar excess of lac repressor over the DNA template to get the maximum yield of RB. Under our experimental conditions, ~90% of the ECs were road-blocked at the lac operator site. And small fractions of ECs escaped the road-block and reached the end of the template, and they were subsequently removed during the washing steps.

For RNase H footprinting, 10 μM concentrations of the antisense oligo (RS663 and RS367 for H-19B and λ N, respectively) were added to the RB for 30 s followed by the addition of 1 unit RNase H and incubated for 1 min at 37 °C. For RNase T1 cleavage assays, 1 unit of enzyme was added to the RB, and the cleavage was continued for 1 min at 37 °C. In both cases, reactions were stopped by phenol extraction, and samples were mixed with equal volume of formamide loading dye and loaded onto 8% sequencing gels.

Inter- and Intramolecular S-S Bond Formation Assays—All the single Cys derivatives of NusA were constructed by site-directed mutagenesis using the Stratagene kit. First, the natural Cys residues of the WT NusA (having 3 Cys residues at positions 251, 454, and 489; pRS523) were removed by introducing the mutations C251S, C454S, and C489S, to make a "zero-Cys" NusA (pRS1100). The single-Cys derivatives, S53C (C53), S29C (C29), and T371C (C371) were made using pRS1100 as a template. V8E-S53C NusA was made by making V8E change on the S53C NusA. The ΔAR1-2 deletion was introduced in the S53C NusA by PCR. All the constructs were made in pET33b plasmid having a heart muscle kinase tag in the N-terminal to be used for end-labeling with ^{32}P. Purification of these NusA derivatives was performed using Ni-NTA beads (Qiagen). The S39C λ N was constructed by site-directed mutagenesis. The natural λ N (having a single Cys at 93; pRS615) was removed by introducing the C93S mutation (pRS1421) to make a zero-Cys λ N. Then the desired S39C change in the NusA binding region was introduced using pRS1421 as a template. S39C λ N was made both in pET21b and pET33b vectors. These single-Cys derivatives of N proteins were purified as described earlier (23).

All the single Cys derivatives of NusA were labeled at their N-terminal heart muscle kinase tag using protein kinase A and [γ-^{32}P]ATP (3000 Ci/mmol). A 10 mM stock of copper-phenanthroline was prepared by adding 1 μl of 1 M $CuSO_4$ and 3 μl of 1 M phenanthroline, and the volume was made to 100 μl by adding water. EC_{23} was chased for 2 min with 250 μM NTPs and 400 nM of different end-labeled single Cys NusA derivatives together with 800 nM of λ N to form the N-NusA modified RB on the T7A1-λ *nutR*-lacO template (amplified from pRS604). The RB was then washed and resuspended in copper-phenanthroline buffer (25 mM Tris-HCl, pH 7.0, 50 mM KCl, 100 mM NaCl). 10 μM copper-phenanthroline was added to the RB and incubated for 10 min, and the reaction was stopped by adding non-reducing SDS loading dye (without β-mercaptoethanol) containing 100 mM iodoacetamide and was loaded onto a 6–10% gradient SDS-PAGE. For the S-S bond formation outside the EC, same amounts of all the other components except RNAP were added to the reaction mixture, and the reactions were performed in the same way as above.

For the intramolecular S-S bond formation assays, WT H-19B N together with indicated double-Cys derivatives of heart muscle kinase-tagged NusA were used. NusA was radiolabeled, and all the other experimental conditions were kept same as above. The highly pure core RNAP was purchased from Epicenter, USA.

RESULTS

N-NusA AR1 Interaction Is Not Important for the Antitermination Process—Earlier it was shown that GST-tagged N proteins from phage λ selectively interacted with the AR1 domain of NusA (Ref. 18; Fig. 1*G*). N-AR1 interaction was further demonstrated by structural analyses (24, 25). All these interactions were demonstrated in the absence of the EC, and hence, the functional significance of N-NusA AR1 interaction was not addressed in these studies (18). Also, it has not been established that this mode of interaction occurs on the surface of the EC during the process of antitermination. We decided to revisit the N-NusA interaction in solution as well as perform detailed analysis to elucidate the functional outcome of this interaction.

At first, we revisited the interactions of N proteins from H-19B and λ phages with the His-tagged full-length and different fragments (having different functional domains) of NusA by measuring the efficiency of each of the fragments to pull down the N proteins in the absence of the EC. We observed differential but significant binding affinity of N for all the NusA fragments as well as to the Ni-NTA-agarose beads. Hence, we were unable to discriminate between specific and nonspecific interactions (data not shown). Other methods of assay also posed similar technical problems with the N proteins. The unstructured nature of N in solution (26) in the absence of RNA and/or RNAP could be a reason for this reduced specificity and its tendency to adsorb on the solid surfaces (beads). It should be noted that N attains specific conformations upon binding to

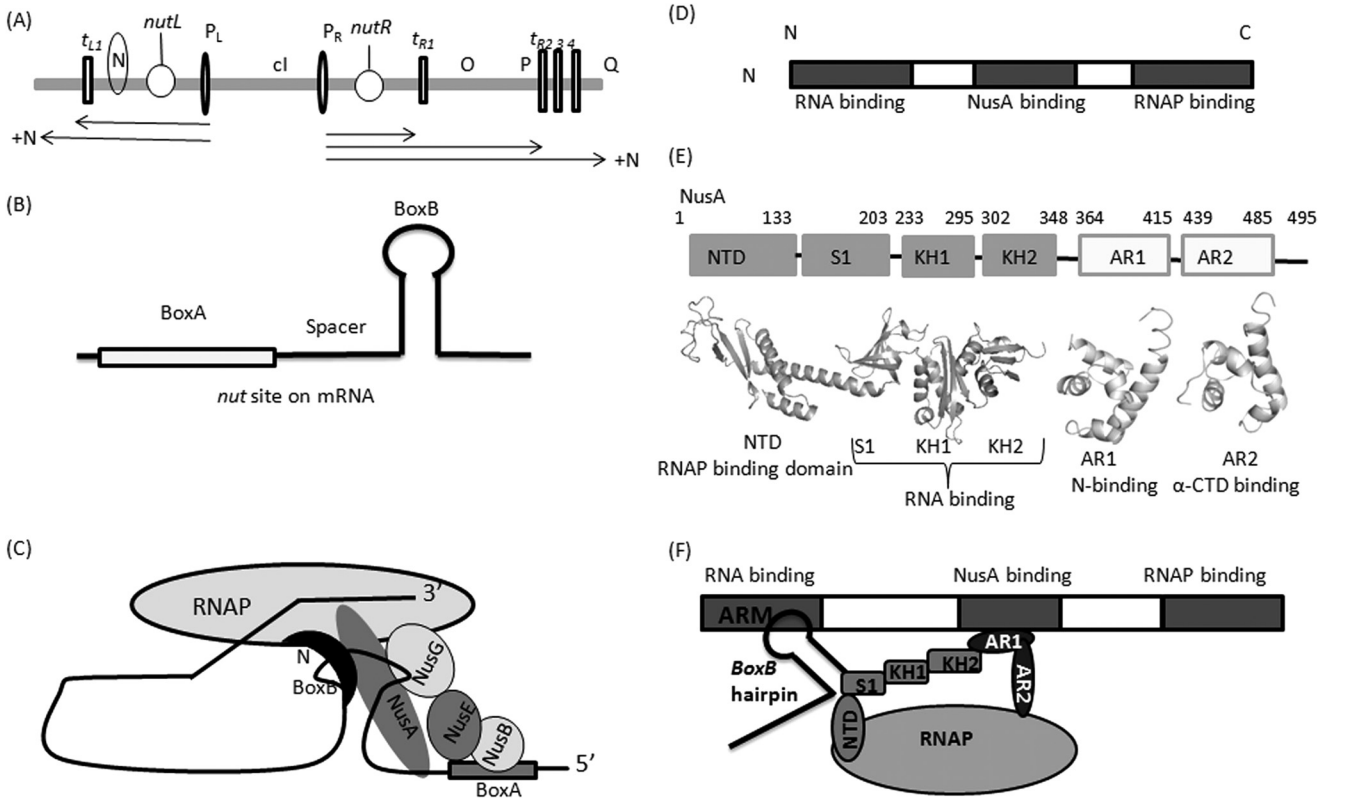

FIGURE 1. *A*, the early region of lambdoid phages. The N gene is indicated. Anti-terminated transcripts in the presence of N are indicated as *bold arrows*. These transcripts originate from P_L and P_R promoters and bypass the t_R and t_L terminators in the presence of N. *B*, the components of the N-binding site, *nut site,* on the mRNA. N recognizes the GNRA tetra-loop of the boxB RNA-hairpin. *C*, schematic showing an EC modified by N and other Nus factors. NusA binds to the spacer, and other Nus factors bind to the boxA region. *D*, N, a small (~12 kDa) basic and unstructured protein that attains structure upon binding to RNA, NusA, and RNAP. Different functional domains are indicated. *E*, different functional domains of 55-kDa NusA. The structural folds of these domains are shown *below the schematic*. *F*, schematic of N-NusA interactions on the elongation complex. According to the published report (18), N interacts with the AR1 region of NusA.

TABLE 2

***In vivo* H-19B N-mediated antitermination assays**

The ratios of β-galactosidase activities in the presence (+ter) and absence (−ter) of terminators give the values of terminator read-through (%RT), which is a measure of antitermination efficiencies. Rho-dependent (P_{lac}-H-19B t_{R1}-*trpt′-lacZYA*; columns 1 and 2) and -independent (P_{lac}-H-19B *nutR*-$T_{R'}$-*T1-T2-lacZYA*; columns 3 and 4) terminator cassettes were fused to the *lacZ* reporter for the assays. The Rho-dependent terminator, t_{R1} was derived from the *nutR-cro* region of phage H-19B. Measurements were performed both in the absence (−H-19B N) and presence (+H-19B) of N proteins. The errors are calculated from the average of 4–9 independent measurements.

nusA alleles	1 +H-19B N β-galactosidase activity			2 −H-19B N β-galactosidase activity			3 +H-19B N β-galactosidase activity			4 −H-19B N β-galactosidase activity		
	+t_{R1}-*trpt′*	−t_{R1}-*trpt′*	%RT	+t_{R1}-*trpt′*	−t_{R1}-*trpt′*	%RT	+$T_{R'}$-*T1-T2*	−$T_{R'}$-*T1-T2*	%RT	+$T_{R'}$-*T1-T2*	−$T_{R'}$-*T1-T2*	%RT
	Arbitrary units			*Arbitrary units*			*Arbitrary units*			*Arbitrary units*		
WT	567 ± 16	933 ± 23	61	19 ± 3	1014 ± 30	1.9	424 ± 26	927 ± 44	46	1.0 ± 0.24	130 ± 6	1.0
ΔAR2	326 ± 14	680 ± 26	48	25 ± 2	1075 ± 51	2.3	423 ± 16	813 ± 12	52	2.0 ± 0.15	143 ± 20	1.4
ΔAR1–2	475 ± 15	913 ± 10	52	16 ± 2	1066 ± 25	1.5	338 ± 6	805 ± 56	42	3.0 ± 0.61	148 ± 6	1.7

mRNA and presumably upon binding to NusA and RNAP that probably induces more specificity in the N-NusA interaction. Therefore, instead of measuring the binding of N with different NusA fragments, we undertook detailed functional analyses to identify the role of C-terminal regions of NusA in the N-NusA complex formation during the process of antitermination.

We compared the effects of the deletions of AR2 and AR1-2 regions of NusA on the *in vivo* antitermination by the N proteins (Tables 2 and 3). We measured the *in vivo* antitermination efficiencies at Rho-dependent (H-19B *nutR*/t_{R1}-*trpt′-lacZYA*, λ *nutR*/t_{R1}-*trpt′-lacZYA*; columns 1 and 2 of Tables 2 and 3, respectively) and at Rho-independent terminators ($T_{R'}$-*T1-T2-lacZYA*; columns 3 and 4 of Tables 2 and 3) from the ratios of β-galactosidase activities obtained in the presence and the absence of the terminators (see "Experimental Procedures" for details). The *lacZYA* reporter fused to these terminator cassettes produced the β-galactosidase activity. We observed that the antitermination efficiency (%RT) of both the N proteins was not affected by the deletions of AR1 and AR2 regions of the NusA. The antitermination was specifically dependent on the presence of the N protein (see the +N columns).

We then performed *in vitro* antitermination assays on the DNA templates having Rho-dependent (t_{R1} terminator; Fig. 2*A*) and Rho-independent ($T_{R'}$-*T1-T2* terminator cassettes; Fig. 2*B*) terminators. As the *in vivo* assays, deletions in AR1 and AR2 regions did not show any effect on the *in vitro* N- mediated antitermination assays. The absence of any effect of AR1 deletion in *in vitro* antitermination assays was also observed earlier

TABLE 3

***In vivo* λ N-mediated antitermination assays**

The ratios of β-galactosidase activities in the presence (+ter) and absence (−ter) of terminators give the values of terminator read-through (%RT), which is a measure of antitermination efficiency. %RT is defined as the same way as in Table 2. Rho-dependent (P_{lac}-l t_{R1}-*trpt′-lacZYA;* columns 1 and 2) and -independent (P_{lac}-l *nutR*-$T_{R'}$-*T1-T2-lacZYA*; columns 3 and 4) terminator cassettes were fused to the *lacZ* reporter for the assays. The Rho-dependent terminator, t_{R1} was derived from the *nutR-cro* region of phage λ. Measurements were performed both in the absence (−λ N) and presence (+λ N) of λ N proteins. ND, not determined.

nusA alleles	1 +λ N β- Galactosidase activity			2 −λ N β- Galactosidase activity			3 +λ N β- Galactosidase activity			4 −λ N β- Galactosidase activity		
	$+t_{R1}$-*trpt′*	$-t_{R1}$-*trpt′*	%RT	$+t_{R1}$-*trpt′*	$-t_{R1}$-*trpt′*	%RT	$+T_{R'}$-*T1-T2*	$-T_{R'}$-*T1-T2*	%RT	$+T_{R'}$-*T1-T2*	$-T_{R'}$-*T1-T2*	%RT
	Arbitrary units			*Arbitrary units*			*Arbitrary units*			*Arbitrary units*		
WT	475 ± 14	944 ± 6	50.3	ND	ND	ND	425 ± 4	891 ± 86	47.7	6.0 ± 1.0	240 ± 9	2.5
ΔAR2	485 ± 30	937 ± 36	51.8	ND	ND	ND	434 ± 10	754 ± 50	57.5	8.0 ± 1.1	379 ± 19	2.1
ΔAR1–2	442 ± 37	824 ± 34	53.6	ND	ND	ND	347 ± 16	890 ± 78	38.9	10.0 ± 1.2	379 ± 18	2.6

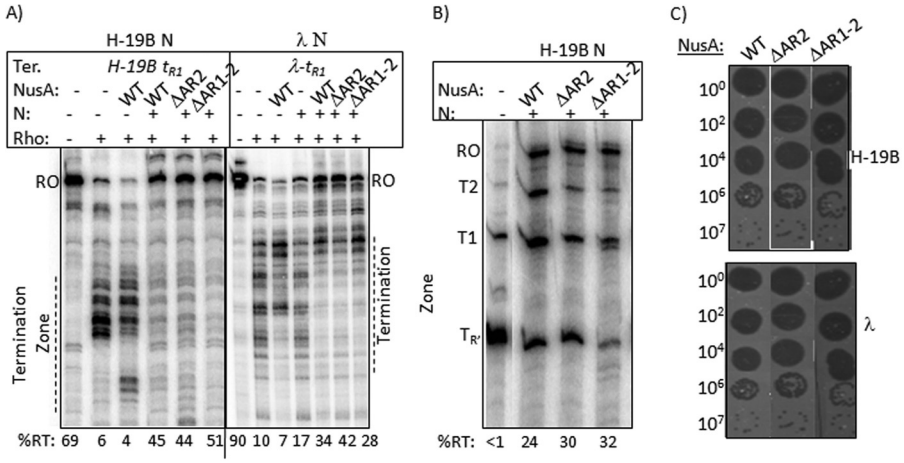

FIGURE 2. **N-NusA AR1 interaction is not required for the antitermination process.** Autoradiograms of the *in vitro* antitermination assays on the DNA templates carrying Rho-dependent (*A;* H-19B t_{R1} and λt_{R1}) and Rho-independent (*B;* $T_{R'}$-T1-T2) terminators in the presence of different NusA fragments. Termination zones and terminated products are indicated. *RO* means run-off product. %RT is defined under "Experimental Procedures." *C*, different dilutions of H-19B and λ phages were spotted on the lawns of MG1655 having indicated derivatives of *nusA* supplied from a plasmid. Different NusA fragments and the source of N proteins are indicated against each figure. The NusA fragments are: WT, full-length; ΔAR2, 1–416 amino acids (amino acid); ΔAR1-2, 1–348 amino acids.

(18). Finally, we observed that the AR1/AR2 deletions did not affect the growths of H-19B and λ phages (Fig. 2*C*).

Therefore, we concluded that the NusA AR1-N interaction during the process of transcription antitermination is not very important, and this interaction may not occur when N-NusA complex is formed on the surface of the EC, and also it is likely that N-NusA binding occurs through another part(s) of NusA. This might happen due to the proposed conformational changes of NusA upon binding to the RNAP (12).

NusA-NTD Mutants Are Specifically Defective for N-mediated Antitermination—The aforementioned results led us to identify the interaction surface involved in a N-NusA complex, when it is bound to the EC. We set-up a genetic screen to isolate NusA mutants defective for N-mediated antitermination. We used a mutagenized library of *nusA* residing on a plasmid and screened for a mutation(s) that caused a antitermination defect of H-19B N at a double-terminator reporter cassette (P_{lac}-*nutR*/t_{R1}-*trpt′-lacZYA*; Ref. 19). This genetic screen yielded only one mutant, V8A. We observed that this mutation is located in a hydrophobic patch of NusA-NTD (Fig. 3*A*). We hypothesized that a hydrophobic surface may take part in the protein-protein interaction. And, hence, we made few more mutations in the nearby hydrophobic amino acids; A7D, V8E, A11D, and V12D. A polar amino acid change, E10K, was also made, but it did not affect the N-antitermination. We also included a previously described mutation, L31E (11), in our assays.

We measured the *in vivo* antitermination efficiency of H-19B and λ N proteins in the presence of these NusA mutants, both at Rho-dependent (Fig. 3, *B* and *D*) and Rho-independent (Fig. 3, *C* and *E*) terminators. We observed that the H-19B N-induced termination read-through was a minimum in the presence of V8E and A11D NusA mutants, whereas only V8E NusA had the most severe effect on the function of λ N. Other mutants also displayed partial defects. Similar trends were observed for both kinds of terminators.

All these NusA mutants were defective in supporting H-19B phage growth (Fig. 3*F*). V8E and L31E mutants showed defects for λ phage growth. These results are consistent with the fact that H-19B N is more dependent on NusA (23, 27). The defects of these mutants were more pronounced in the case of phage growth, because the latter requires more stable and processive interactions between N and NusA.

Next, we measured the *in vitro* antitermination efficiencies (%RT) of H-19B N and λ N using two DNA templates, one having Rho-dependent terminators (H-19B t_{R1}-*trpt′*, a fusion of two terminators, and λ t_{R1}; Fig. 4, *A*, *B*, *E*, and *F*) and another with a Rho-independent triple terminator cassette ($T_{R'}$-*T1-T2*; Fig. 4, *C* and *D*). These NusA mutants caused severe defects to

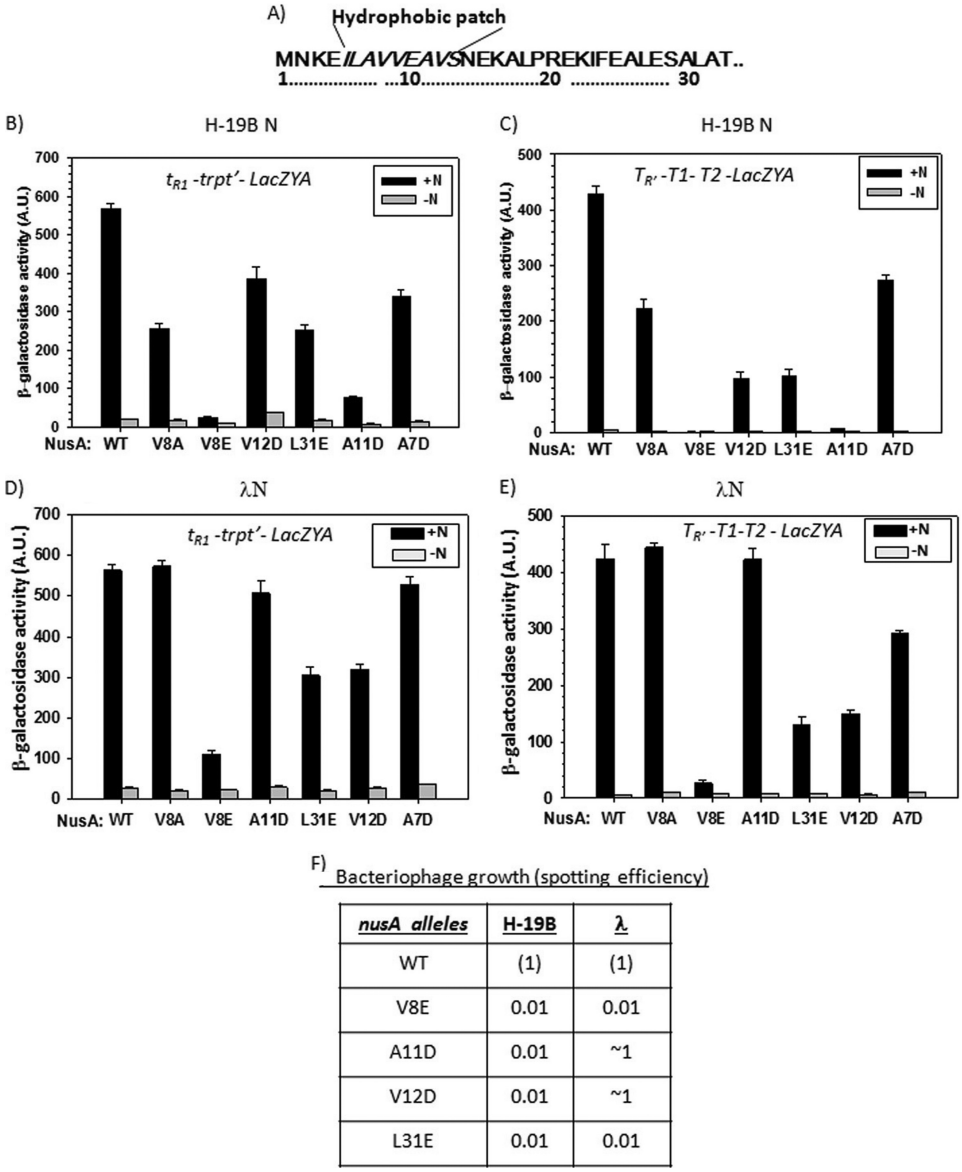

F) Bacteriophage growth (spotting efficiency)

nusA alleles	H-19B	λ
WT	(1)	(1)
V8E	0.01	0.01
A11D	0.01	~1
V12D	0.01	~1
L31E	0.01	0.01

FIGURE 3. **Point mutations in NusA-NTD impair N-antitermination *in vivo*.** *A*, the amino acid sequence surrounding the hydrophobic patch (*italics*) of the NusA-NTD. The *numbering* indicates the amino acid positions from the N terminus of NusA. The *bar diagrams* show the β-galactosidase activities from the reporter cassettes having Rho-dependent (*B* and *D*) and Rho-independent (*C* and *E*) terminators in the presence of the NusA-NTD mutants. Values obtained both in the absence and presence of H-19B N and λN are shown, and the comparison of −N and +N values gave the measure of *in vivo* antitermination. *F*, phage spotting efficiencies in the presence of the NusA-mutants. Experimental conditions were same as in Fig. 2*C*. Efficiency in the presence of WT NusA was set as 1. *A.U.*, arbitrary units.

the N antitermination on the triple terminator cassette, and the effect was milder at the Rho-dependent terminators. Like *in vivo* assays, the V8E NusA also showed the most severe effect on the *in vitro* antitermination activities of H-19B and λ N proteins. It should also be noted that under our experimental conditions, λ N alone was unable to bring about antitermination (Fig. 4*E*, *fourth lane from left*).

These NusA-NTD mutants did not affect the cell viability (Fig. 5*A*). They were not defective for transcription-pausing at His-pause sequences (data not shown) and for the termination enhancement activities at the NusA-dependent $T_{R'}$ terminator *in vitro* (data not shown). These results indicate that the aforementioned mutations in NusA-NTD do not affect RNAP or RNA binding. The CD spectra of all these mutants also revealed that the mutations did not cause significant changes in the secondary structures (data not shown). As these mutations did not affect the other functions of NusA (RNAP binding, termination etc., described above) as well as the viability of the cell (Fig. 5*A*), we can assume that the mutations might not have affected the tertiary structures of the proteins significantly. Therefore, the defects caused by these mutations are specific for N-mediated antitermination and are not due to the changes in NusA conformations.

We localized these mutants both on the homology model of the *E. coli* NusA and on the NMR structure of NusA-NTD (Fig. 5, *B* and *C*) and observed that the mutants are clustered in and around a hydrophobic convex surface of the NusA-NTD. Interestingly, this surface of NusA is located opposite its concave RNAP binding surface (Fig. 5*C*; Ref. 11). It should be noted here that we have mainly tested the roles of hydrophobic amino

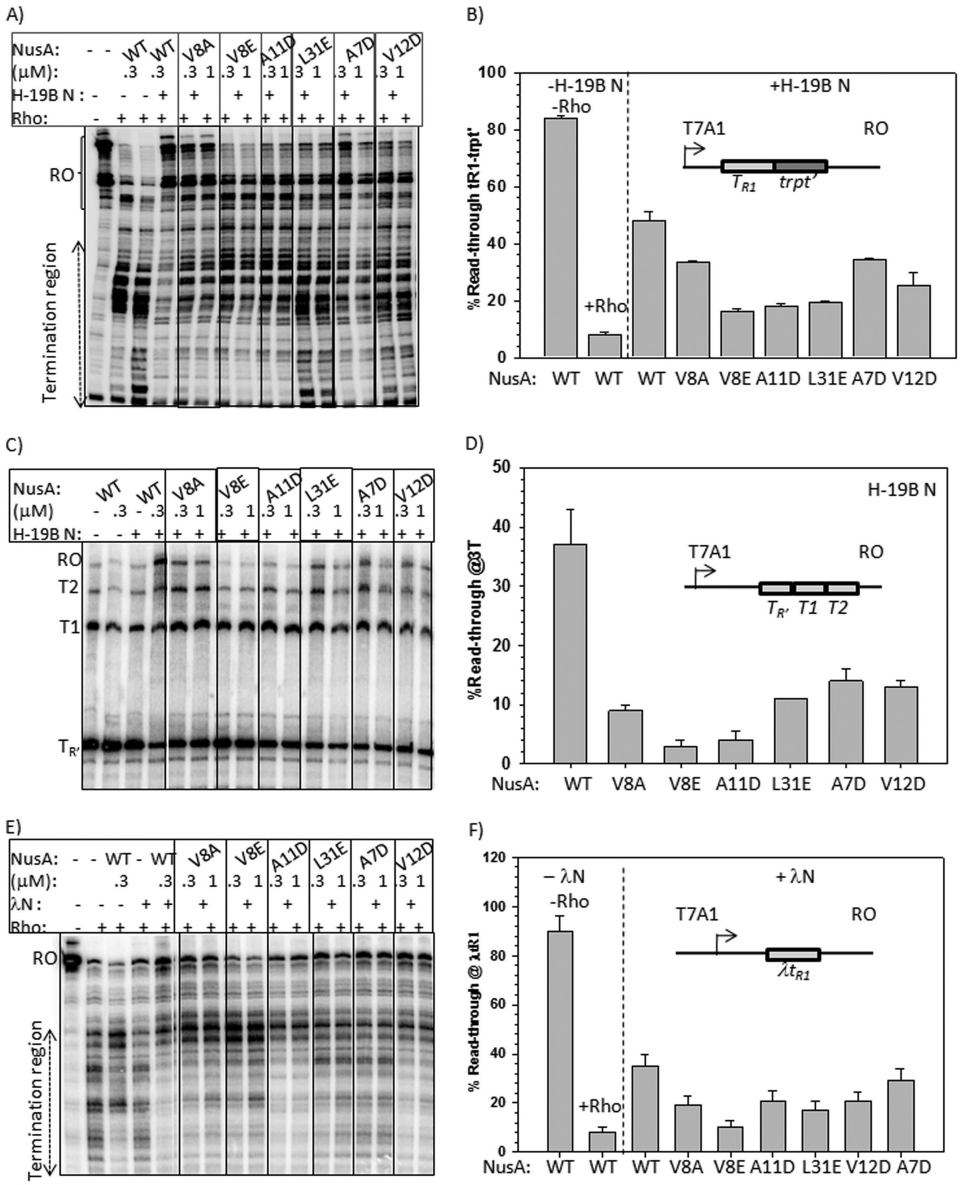

FIGURE 4. **NusA-NTD mutants affect *in vitro* antitermination.** Autoradiograms of *in vitro* transcription termination assays on the templates having H-19B *nutR/*t_{R1}*-trpt'* terminators (*A*), $T_{R'}$*-T1-T2* terminators (*C*), and λ t_{R1} terminator (*E*) in the presence of WT and NusA mutants with WT H19B-N and λ N. Rho was added for Rho-dependent terminators in *A* and *E*. Termination regions are indicated by *double arrowed dotted lines next to the transcript bands*. At the Rho-independent terminators, specific terminated products are indicated. *RO* denotes the run-off product. Concentrations of DNA template, RNA polymerase, N, Rho, and NusG were 5, 25, 100, 50, and 200 nM, respectively. Samples were run on an 8% sequencing gels for the templates with Rho-dependent terminators, and that for Rho-independent terminators 6% gel was used. *Bar diagrams* show the average of read-through efficiencies (% Read-through), those calculated from the *in vitro* N-induced antitermination assays both at the Rho-dependent (*B* and *F*; *H-19Bt*$_{R1}$*-trpt'* and λt_{R1}) and -independent (*D*) terminators in the presence of the different NusA mutants. Formulae used for the calculations are given under "Experimental Procedures." The *errors* were obtained from three measurements.

acids so we cannot rule out the involvement of the polar amino acids of this region in the interaction process. As the same mutations of NusA affected the antitermination functions of two distantly related N proteins (23) from H-19B and λ phages, it is likely that this mode of N-NusA interaction is conserved among different N proteins.

Other NusA mutants defective for λ phage growth were reported in the literature (L183R, Ref. 28; R199A, Ref. 29; G253D and G219D, Ref. 30) and were implicated in the process of N-mediated antitermination. However, all of them are in the NusA-RNA binding domains (SKK domain) and are likely to be defective in binding to the spacer region of the *nut* site of the nascent RNA (31).

NusA-NTD Mutants Impaired N-boxB Interactions in a Stalled EC—Next we tested whether these NusA-NTD mutants affected the N-NusA interaction when the complex is bound to the EC. Binding of H-19B N to the *boxB* of the *nut* site is highly dependent on its interaction with NusA, which is bound to the adjacent spacer region (Fig. 1). Therefore, we used binding of H-19B N to the *boxB* region as a measure of N-NusA interaction at the *nut* site of the EC. We stalled an EC downstream of the *nut* site using lac repressor as a road block (Fig. 6*A*). We footprinted the *nut* site of the nascent RNA in the presence of H-19B N and different derivatives of NusA using RNase T1 and RNase H. In these assays protection of the *nut* site indicates binding of N as well as N-NusA interaction at this site (19).

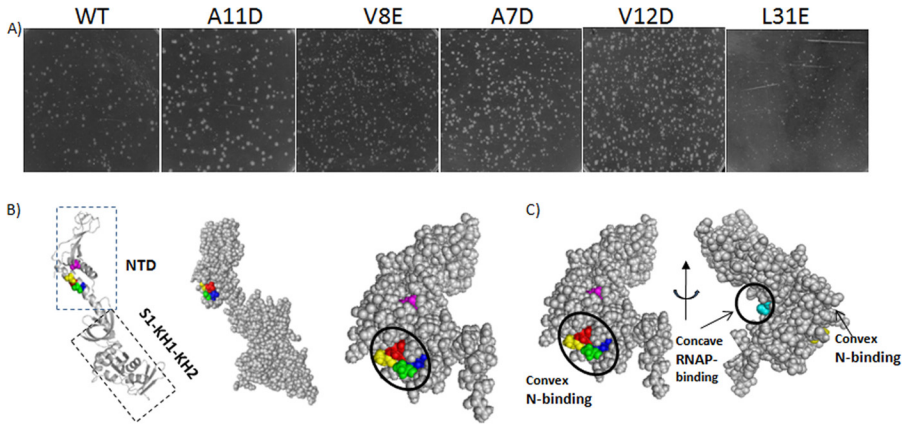

FIGURE 5. *A*, cell viability assays of NusA mutants. MG1655*rac*$^+$ strains were transformed with pHYD3011 having WT and mutant *nusA,* and then the viable transductants were obtained by moving *nusA*::*Cam*^{R} through P1 transduction. Transductants were plated on LB media. Except L31E, all were as healthy as WT. L31E NusA produced smaller transductants. This defect of L31E could arise from its impaired RNAP binding property (11). *B*, locations of these mutants are indicated on the homology model of *E. coli* NusA (1–348 amino acids). Defective mutants are indicated in different colors as; A7D in *yellow*, V8E in *red*, A11D in *green*, V12D in *blue*, and L31E in *magenta*. Mutations are also shown on the NMR structure of NusA-NTD with the same color coding (PDB code 2KWP; *third from the left*). *C*, NMR structure of the *E. coli* NusA-NTD showing the convex putative N-binding surface and the concave RNAP-binding surface. Ser-29, shown in *sky blue color*, is important for interacting with RNAP. All the structures were drawn using the academic version of the PyMOL.

Three G residues in the *nut* site (see the −*N lanes* of Fig. 6, *B* and *C*, indicated by a *dashed line*; 19) are sensitive to RNase T1. We monitored the protection of these G residues under different conditions (Fig. 6, *B* and *C*). We observed the following. 1) The N-NusA mediated protection of the *nut* site was observed in the presence of WT, ΔAR1-2, and ΔAR2 NusA proteins (Fig. 6*B*). 2) This protection was missing in the absence of N and NusA and in the presence of N with NusA-NTD mutants V8E and A11D (Fig. 6*C*). It should be noted that under our experimental conditions, H-19B N alone was unable to provide any protection (data not shown).

Then we repeated the same footprinting assays using RNase H. An oligo, RS663, antisense to the spacer region, was used to induce the RNase H cleavage. RNase H cleavage will be absent if the antisense oligo is prevented from binding to this site because of the presence of N and NusA. We observed a significant reduction in RNase H sensitivity when WT, ΔAR1-2, and ΔAR2 NusA proteins were present (Fig. 6*D*). The RNase H cleavage was observed in the presence of NusA-NTD mutants (Fig. 6*E*). These results were consistent with the RNase T1 footprinting (Fig. 6, *B* and *C*). A similar protection pattern as H-19B N was also observed when the experiments were performed with λ N modified stalled ECs using a template having the λ nut site (data not shown). These results indicated that ΔAR2 and ΔAR1-2 derivatives of NusA do not affect N binding to the *nut* site, whereas the NusA-NTD mutants V8E and A11D do this severely. As the N-*nut* interaction is highly dependent on the functional N-NusA interaction at this site, we concluded that NusA-NTD mutants, and not the AR1/AR2 deletions, perturbed the N-NusA complex formation.

A Cys Residue in the Convex Surface of NusA-NTD Forms the S-S Bridge with Another Cys Residue from the NusA Binding Region of λ N—The functional analyses of the different mutants at the convex surface of the NusA-NTD (Figs. 3 and 4) and the N-NusA interaction analyses using RNase footprinting (Fig. 6) showed that these residues of NusA-NTD play an important role in N-NusA interaction during transcription elongation. Next, we attempted to demonstrate the physical proximity of this region of NusA to N when the complex is formed on the EC. We have chosen λ N for these assays because its NusA binding region is well characterized (8). Cys-Cys disulfide bridge (S-S bridge) formations between different regions of N and NusA were employed to demonstrate the proximity of the regions. This bridge is formed only if the interacting partners come within ~6 Å.

We constructed single Cys derivatives of NusA: S29C and S53C (in the NusA-NTD domain) and T371C (in the AR1 domain) (see Fig. 7, *A* and *B*). These single Cys derivatives were introduced after removing the three natural Cys residues of NusA. The rationale for introducing Cys residues at these positions is as below. 1) Cys-53 is located near the convex surface (~10 Å) where all the NusA mutants defective for N-function are localized (Fig. 5). 2) Cys-29 is situated at the opposite concave surface of NusA (Fig. 7*A*) and was shown to interact with RNAP (11). Due to its location at the surface opposite to the putative N-interaction region, we used this substitution as a negative control. 3) T371C substitution, located within the interacting distance of the N peptide in the peptide-NusA AR1 complex (Fig. 7*B*), was chosen to probe NusA AR1-N interaction, if any, in the presence of the EC. 4) We have chosen to replace naturally occurring Ser or Thr residues with Cys for minimizing the effects on the proteins. 5) The space-fill models of different domains of NusA indicate that these Cys residues are surface-exposed (Fig. 7, *A* and *B*).

We introduced a S39C (39C) mutation in the NusA binding region of λ N (amino acids 34–47; Fig. 7*B*; Refs. 8 and 24) after removing the single naturally occurring Cys from the protein. In the AR1-N peptide complex, Cys-39 is located near the Cys-371 of NusA-AR1 region (Fig. 7*B*).

These single Cys derivatives of both the NusA and N were functional in the *in vitro* transcription antitermination assays both at Rho-independent (Fig. 7*C*) and -dependent (Fig. 7*D*) terminators. Also, the mutations did not affect their secondary structures significantly (data not shown). We formed the λN-NusA complex both in the absence of the EC (Fig. 8*A*) and on the surface of a stalled EC (Fig. 8*B*). The stalled EC modified

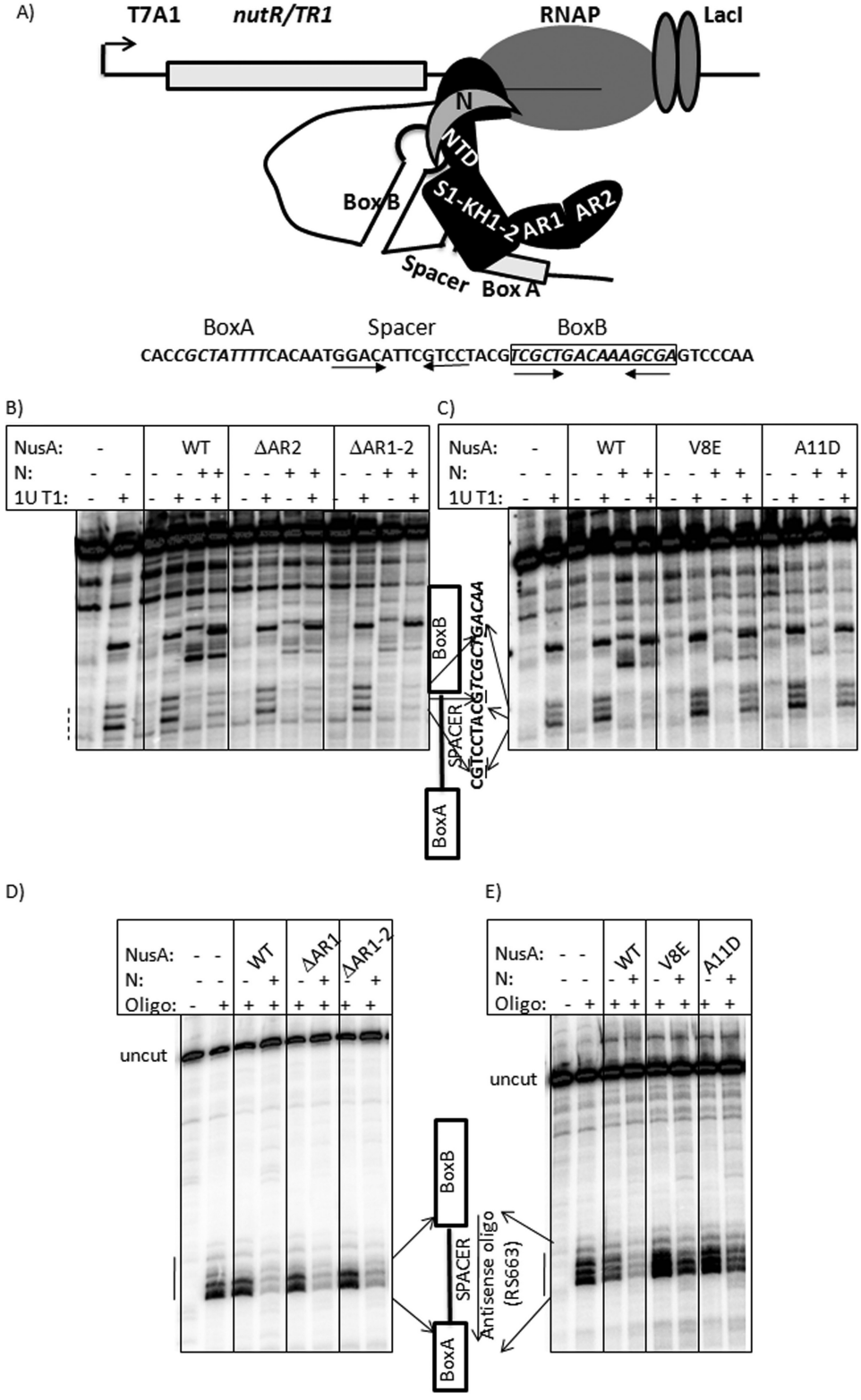

FIGURE 6. **Nus-NTD mutations disrupted N-NusA-nut site interaction.** *A*, a schematic showing an H-19B N/NusA-modified EC stalled by the lac repressor. Different domains of NusA are *highlighted*. Detailed sequence of the H-19B *nut* site is shown *below the schematic*. *B* and *C*, RNase T1 footprinting of the *nut* RNA of the stalled EC modified with H-19B N together with WT and different derivatives of NusA as indicated. The *nut* site is indicated. The three RNase T1-sensitive G residues are shown. *D* and *E*, RNase H footprinting of the same *nut* RNA as above. An oligo (RS663), antisense to the spacer region, is indicated. Other experimental conditions were same as in *C*.

with N and NusA was formed in a similar way as described in Fig. 6*A*, except that the DNA template used in these experiments had a λ *nut* site with the *lac* operator sequence placed just downstream of it (amplified from pRS604). The N-NusA complex in Fig. 8*A*, was formed with the same components as described in Fig. 8*B*, except that RNAP was omitted from the

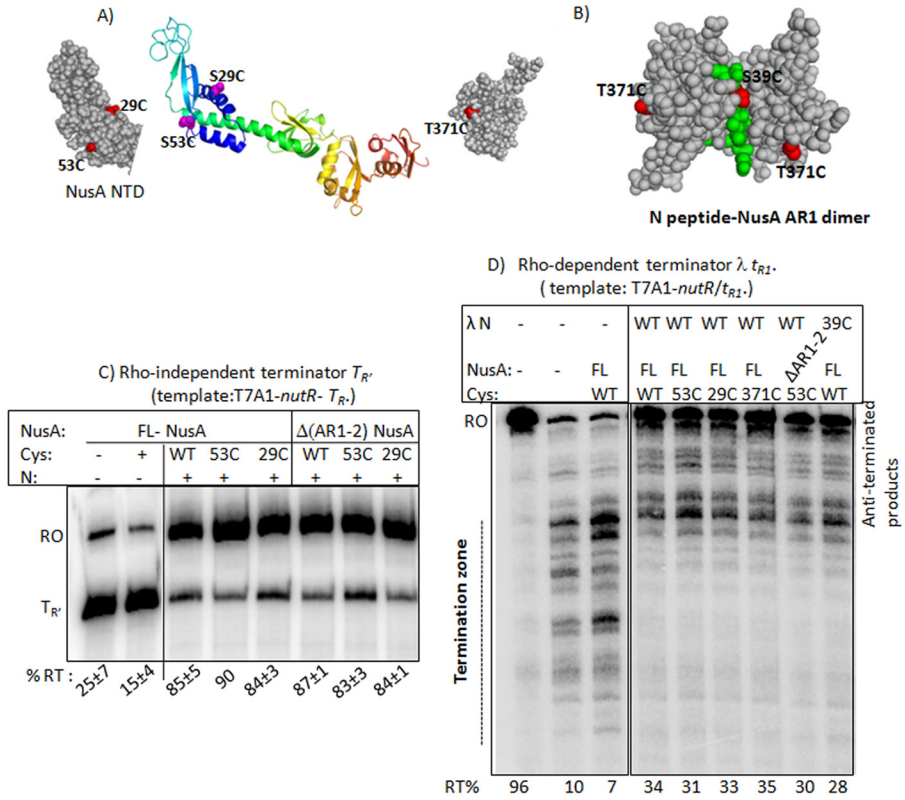

FIGURE 7. **Activities of the single Cys derivatives of NusA and λ N.** *A* and *B*, locations of the cysteines on the homology model of *E. coli* NusA and the structure of N (34–40) peptide (*green thread*) complexed with AR1 dimer (PDB code 1U9L). A part of NusA-NTD is shown as *space-filled* to highlight the concave and convex curvatures. *Space-fill models* also revealed that Cys residues are surface-exposed. *In vitro* transcription antitermination assays at Rho-independent $T_{R'}$ (*C*) and Rho-dependent λt_{R1} (*D*) terminators with different combinations of NusA and N derivatives are shown. 50 nM Rho was added to all the lanes except the *left-most lane*. DNA templates and reaction conditions were the same as described in Fig. 4. %RT in *C* was calculated as ([RO]/{[RO] + [$T_{R'}$]}) and that in D as ([RO]/{[RO] + [all the terminated transcripts]}).

reaction. We induced S-S bridges by using an oxidizing agent, copper-phenanthroline. The same experiments were also repeated in the absence of λ N (*right panels* of Fig. 8, *A* and *B*). Radiolabeled NusA proteins were used to monitor the different S-S-bonded species. We identified the N-NusA complex (N-NusA) and the NusA dimer ($NusA_2$) by comparing their migrations with the molecular weight markers. The N-NusA complexes were further confirmed by their absence in the −Cys-39 (−*39C*) N panels (*right panels* of Fig. 8, *A* and *B*). These species were indeed S-S-bonded, as was evident from their disappearance in the presence of a reducing agent, DTT (see the +*DTT* lanes in all the panels of Fig. 8, *A* and *B*), and by their absence when Zero-Cys (*No Cys*) NusA was used (*lanes 1–3* of Fig. 8, *A* and *B*). The presence of N in the N-NusA species was confirmed by repeating some of the experiments with radio-labeled N (data not shown).

The maximum amount of N-NusA species (~23%) was formed between Cys-371 NusA (in the AR1 domain) and Cys-39 N, when the complex was formed in the absence of the EC (Fig. 8*A*, *lanes 10–12*), which is consistent with the fact that NusA-AR1 domain specifically interacts with N in solution (18). Formation of this species was negligible when ΔAR1-2 NusA instead of full-length NusA was used (*lanes 16–18*). Lesser amounts of N-NusA species were also seen in the presence of Cys-29- and Cys-53-NusA, which could arise from the inherent nonspecific nature of N-NusA interaction in the absence of the EC.

Interestingly, when the N-NusA complex was bound to the stalled EC (Fig. 8*B*), a significant amount of S-S bridge was observed between Cys-39 N and Cys-53 NusA (~20%; *lanes 7–9*) instead of Cys-371 NusA (*lanes 10–12*). S-S bridge formation was absent in the presence of Cys-29 NusA. A significant amount of this Cys-39 N-Cys-53 NusA species was also observed with ΔAR1-2 NusA (*lanes 16–18*), and this species was absent when V8E NusA, defective for N-antitermination, was used (*lanes 13–15*). It should also be noted that a lower level of S-S bond formation between NusA-Cys-53 and N- Cys-39 was observed in the N-NusA binary complexes under different conditions (Fig. 8*A*; 5.5% in *lane 8*, 5.0% in *lane 14*, and 3.0% in *lane 17*). This may indicate an intrinsically higher reactivity of NusA- Cys-53.

Therefore, on the surface of the EC, specific S-S bond can form between the Cys-39, located in the NusA binding region of λ N (34–47 amino acids), and the Cys-53 of the NusA-NTD. This bond formation occurred due to the specific NusA NTD-N interaction because V8E NusA was unable to form the S-S bridge, and the latter was also missing when Cys-29 or Cys-371 NusA proteins were present. These results strongly indicated that upon binding to the EC, the interaction surface of NusA for N, changes from its AR1 region to the NTD domain. And residues at the convex surface of this domain play an important role in this interaction.

We would like to point out the formations of N-induced NusA dimers between Cys-53 residues when bound to the sur-

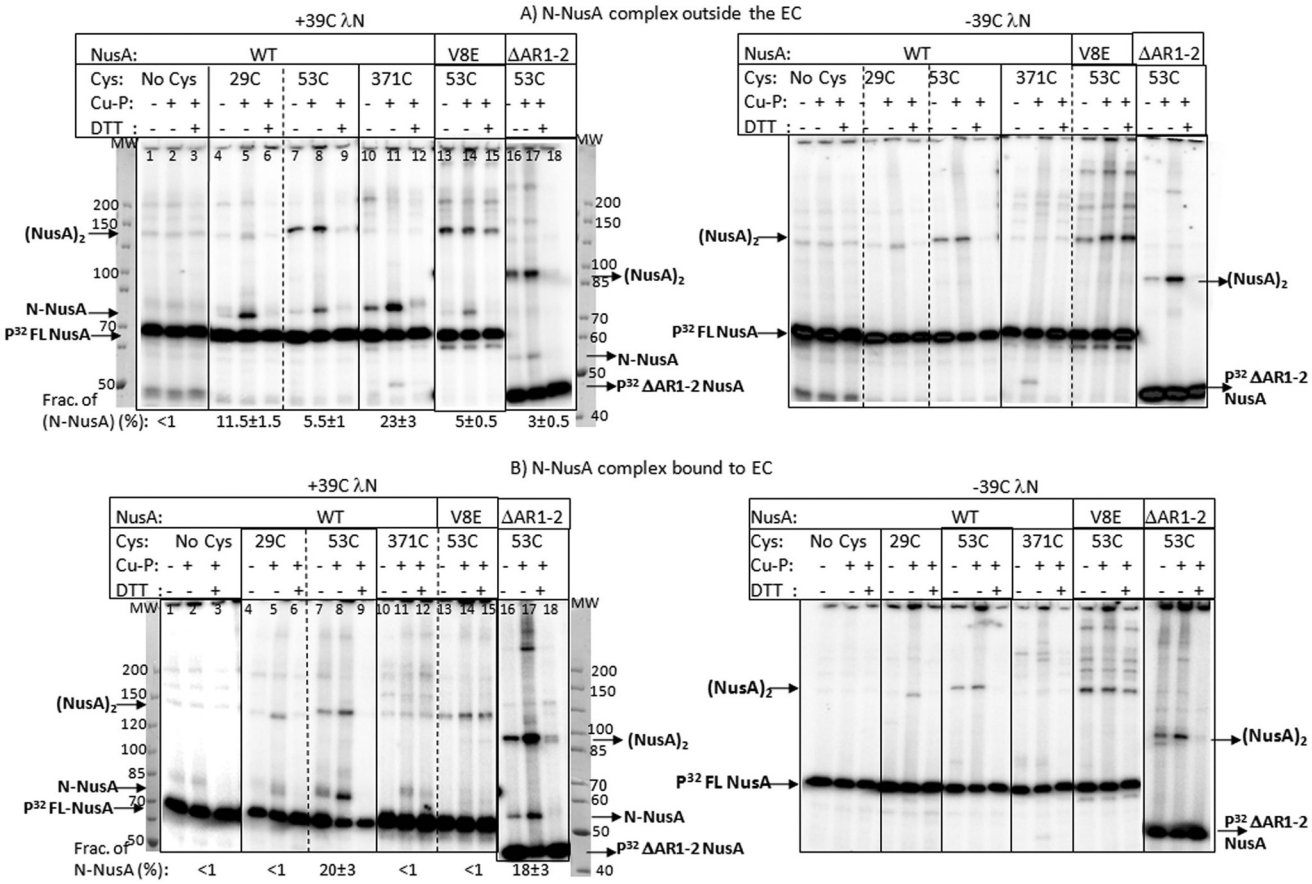

FIGURE 8. **S-S bridge formation between Cys-39 of λN and the single Cys derivatives of NusA.** *A*, autoradiogram of the end-labeled WT and different NusA derivatives both in the presence (+*39C N*, *left panel*) and absence (−*39C N*, *right panel*) of Cys-39 λN. The N-NusA binary complex was formed outside the EC in the absence of RNAP. *B*, N-NusA complex formed on the stalled EC in the presence (+*39C N*, *left panel*) and absence of N (−*39C N*, *right panel*). ECs in these experiments were formed in a similar way as described in Fig. 6*A*. Different S-S-bonded species in all the panels are indicated. *MW*, molecular weight markers, which were loaded together with other lanes and were separately stained with Coomassie Blue dye and later aligned with the autoradiograms. The fractions of N-NusA complex indicated *below the lanes* were calculated as ([intensity of N-NusA]/intensities of [unreacted species] + [N-NusA] + [$NusA_2$])%. Errors were estimated from at least three measurements.

face of the EC under different conditions (*lanes 7*, *8*, *13*, *14*, *16*, and *17* of Fig. 8, *A* and *B*). The presence of two copies of NusA in a N-NusA-modified EC, having two different functions, was hypothesized earlier (14). Further experimentations are required to understand the functional significance of this N-induced NusA dimer in the antitermination process.

AR1/AR2 Regions of NusA Stay Away from N in the EC—Inhibition of RNA binding function of NusA by its own AR2 domain (12) and capability of the latter to interact with the SKK domains in *trans* (32) suggest that AR2 folds over the SKK domain forming a "closed state" NusA in solution (Fig. 9*A*). This autoinhibition is removed when NusA interacts with the EC, likely by forming an "open state" (Fig. 9*A*). However, the existence of these states has not been confirmed experimentally. Moreover, the shifting of the NusA interaction surface for N from AR1 to the NTD domain could be a consequence of the EC-induced conformational changes of NusA. Hence, we investigated the spatial orientation of the AR1/AR2 regions of NusA when it is a part of N-NusA-EC ternary complex.

We used a NusA having a pair of Cys residues at 251 (in SKK domain) and at 489 (in AR2 domain) positions. This pair is likely to form a S-S bridge if AR2 folds over the SKK domain. We induced the intramolecular S-S bond by copper-phenanthroline and measured the intramolecular species (C-C) formation of NusA under three different conditions; (i) when it is in solution, (ii) when it is bound to the core RNAP, and (iii) when it is bound to a stalled EC. The state of NusA in each of the cases was measured both in the absence and presence of H-19B N. N-NusA-modified stalled EC was formed in the same way as described in Fig. 6*A*.

Consistent with the closed state hypothesis, ~50% of the NusA molecules underwent Cys-489--Cys-251 pairing (C-C NusA) in solution (*outside EC panel*, Fig. 9*B*, *lane 2*), which indicated that AR2 indeed folds over the SKK domain. In the presence of N, the amount of C-C NusA was reduced but was still significant (*lane 5*). This reduction could be due to the formation of N-induced intermolecular S-S bridges between NusA molecules (higher molecular weight bands). Interestingly, similar results were also observed in the presence of core RNAP (+*core RNAP panel*, Fig. 9*B*, *lanes 13–18*). This indicates that the α-subunit of the core RNAP in solution does not alter the closed conformation of NusA. When NusA was bound to the EC, AR2 did not form Cys-Cys bonding with SKK domain (*Inside EC panel*, Fig. 9*B*, *lane 8*), as indicated by the drastic reduction of the amount of C-C species. The presence of N in the ternary N-NusA-EC complex did not induce the bond for-

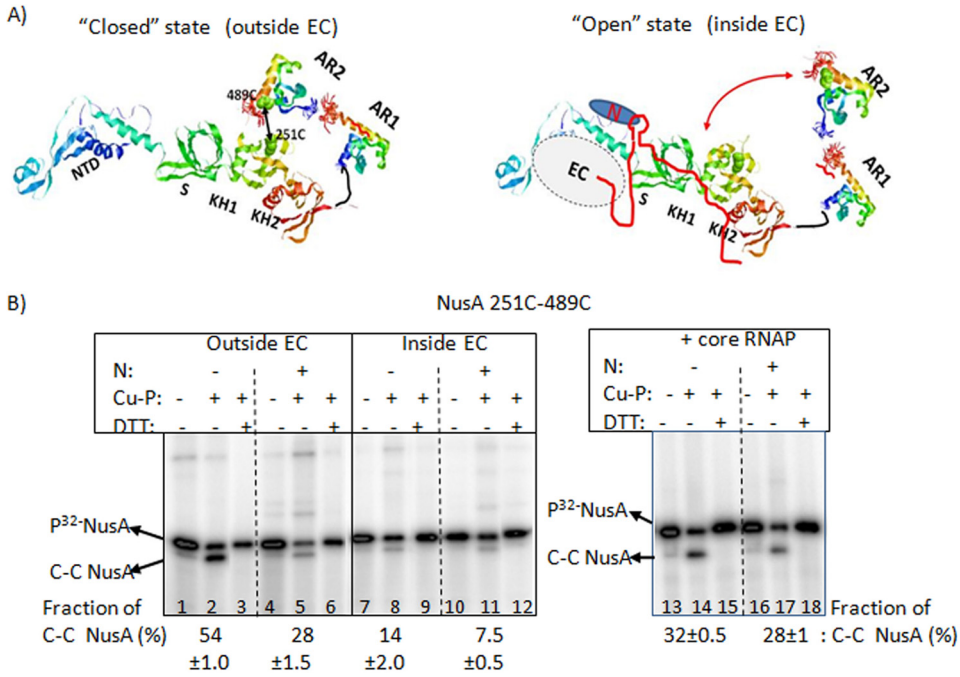

FIGURE 9. **Intramolecular cross-linking of NusA.** *A*, the NMR structures of AR1 (PDB code 1WCL) and AR2 (PDB code 1WCN) were added to the homology model of *E. coli* NusA manually, and hypothetical closed and open states are depicted. The possibility of occurring Cys-Cys pairing (*double-sided arrow*) between Cys-489 (*489C*) of AR2 and Cys-251 (*251C*) of SKK domains is shown in the closed state. *B*, autoradiograms of the ^{32}P-labeled NusA shown under different conditions. Experiments were performed in the same way as in Fig. 8. C-C NusA indicates the intramolecular S-S-bonded species. Fractions of the C-C NusA shown below was calculated as [C-C NusA]/{[C-C NusA] + [NusA]}. In all these experiments, H-19B N was used. In the +*core RNAP panel*, NusA was mixed with 100 nM core RNAP in the same buffer. Immobilized DNA template was not added in the core RNAP experiments.

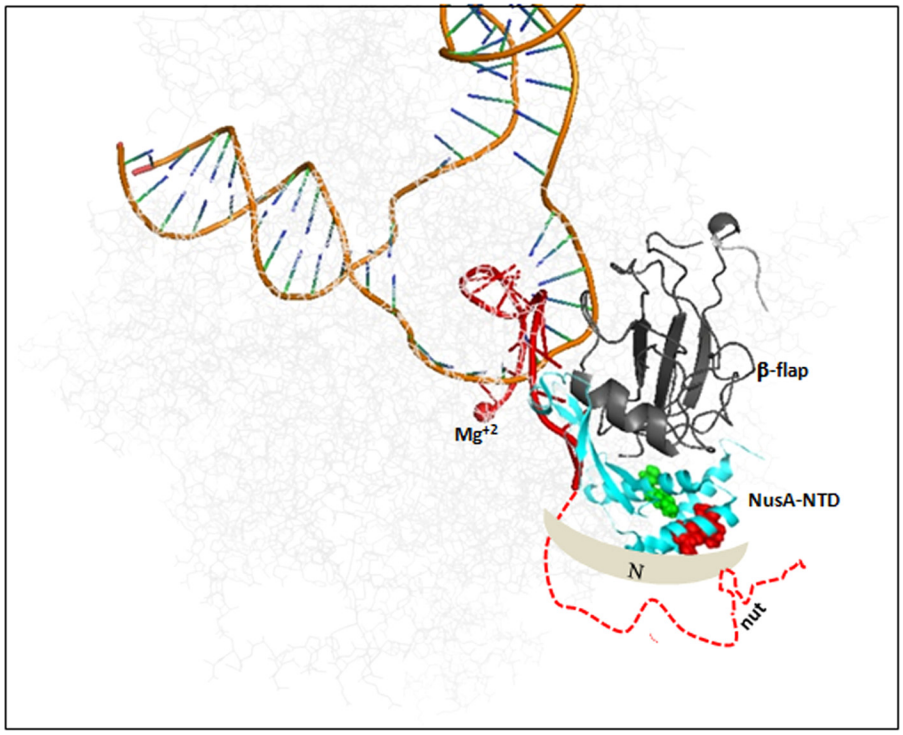

FIGURE 10. **A possible model of the N-NusA NTD-EC ternary complex (37).** Exiting RNA (*red*), β-flap (*dark gray*), and NusA-NTD (*cyan*) are *highlighted*. The rest of the β/β′ are shown in *light gray*. N is shown as a schematic. N and RNAP binding residues of NusA-NTD are in *red* and *green spheres*, respectively. The RNA outside the EC is shown as a *dotted line*.

mation either (*lane 11*), which would have been expected if the N-AR1 interaction occurred on the surface of the EC. This also suggests that the AR1 region of NusA stays away from the EC even in the presence of N.

The above results confirmed that NusA undergoes drastic conformational changes upon interaction with EC, where the AR2 region stays away from the SKK domain, forming the open state (Fig. 9*A*). As AR1 domain is adjacent to the AR2, it is likely

that this domain also stays away from the SKK domain in this configuration. In the N- and NusA-modified EC, N is located at the boxB of the *nut* site, which is adjacent to the SKK domain of the spacer-bound NusA. And hence, in the open conformational state, *i.e.* on the surface of the EC, NusA-AR1 fails to make any contact with N due to the conformational constraints.

DISCUSSION

Based on the following evidences, we concluded that a hydrophobic patch of the NusA-NTD convex surface (Fig. 5, *B* and *C*), and not the NusA-AR1 domain, is the interaction site for N during the process of antitermination. 1) Point mutations in this convex surface specifically impaired the N-antitermination process (Figs. 3 and 4). 2) These mutants perturbed the N-NusA interaction at the *nut* site of the nascent RNA, which in turn affected their binding to the spacer boxB elements (Fig. 6). 3) An engineered Cys residue located near this hydrophobic patch of NusA specifically formed an S-S bridge with an engineered Cys in the NusA binding region of the N protein (Fig. 8). 4) Deletions of AR1 and AR2 regions of NusA in any of the aforementioned assays did not have any effect. 5) Finally, a massive away-movement of NusA AR1-2 regions upon binding to the EC (Fig. 9) most likely makes this region inaccessible to the boxB-bound N during the process of antitermination.

NusA-NTD intrinsically does not have high affinity for N (18). However, this region becomes the preferred binding site for N when N and NusA are part of the EC. We suggest the following reasons for this. 1) The hydrophobic amino acids provide an ideal groove for the thread-like (24) NusA binding region of N. 2) The affinity of NusA-NTD fragment for N increases in the open state of NusA when it is bound to the EC. 3) Finally, it is also possible that this interaction takes place due to the physical proximity of the NusA-NTD to the *nut* site as well as to its SKK domain in the N-NusA modified EC (Fig. 10).

This N binding region of NusA-NTD is located opposite its concave RNAP binding surface (Fig. 5*C*) and lies within a distance of ~20 Å. This proximity is ideal for N to exert conformational changes in and around the NusA-binding sites, the β-flap/β'-dock regions of the RNA exit channel (Refs. 10 and 11; Fig. 10) of the EC, allosterically via NusA. This altered interactions of NusA with the RNA exit channel is likely to stabilize the interactions between the exiting RNA and the channel and that between the clamp domain and the DNA template, which are the important factors for enabling the antitermination. Hence, the N-NusA NTD interaction at the *nut* site holds the key to convert the transcription termination factor, NusA, into an antiterminator. Detailed analyses of N-induced altered interaction patterns of NusA on the EC is required to further understand the mechanism of this conversion.

We have earlier shown that RNAP mutations in and around the RNA exit channel perturb N action (23) and also proposed that the N C-terminal domain may penetrate into the core of the EC through this exit channel (33). Here, we propose that in addition to N-EC direct interactions, N-NusA NTD binding also affects the adjacent β-flap regions. The antiterminator, Q, has been shown to modify the NusA-EC interaction in such a way that it forms an extended shield on the RNA exit channel (34). The unique *cis* acting antiterminator, the PUT RNA, interacts with β'-zinc finger motif present near the same RNA exit channel (35). Involvement of NusA in PUT action has not yet been proven but also is suspected. A recently described antiterminator protein, gp39, has been shown to target the RNA exit channel of the EC (36). As the RNA exit channel is the site where the hairpin-terminators are formed and through which the terminator protein, Rho, approaches the interior of EC (1), it is quite logical that the mode of action of the antiterminators has evolved to target the same site.

Acknowledgments—We thank Prof. Max Gottesman for critically reading the manuscript. We also thank other laboratory members for critically proofreading the manuscript.

REFERENCES

1. Peters, J. M., Vangeloff, A. D., and Landick, R. (2011) Bacterial transcription terminators. The RNA 3′-end chronicles. *J. Mol. Biol.* **412,** 793–813
2. Banerjee, S., Chalissery, J., Bandey, I., and Sen, R. (2006) Rho-dependent transcription termination. More questions than answers. *J. Microbiol.* **44,** 11–22
3. Santangelo, T. J., and Artsimovitch, I. (2011) Termination and Antitermination. RNA polymerase runs a stop sign. *Nat. Rev. Microbiol.* **9,** 319–329
4. Weisberg, R. A., and Gottesman, M. E. (1999) Processive antitermination. *J. Bacteriol.* **181,** 359–367
5. Chattopadhyay, S., Garcia-Mena, J., DeVito, J., Wolska, K., and Das, A. (1995) Bipartite function of a small RNA hairpin in transcription antitermination in bacteriophage λ. *Proc Natl. Acad Sci. U.S.A.* **92,** 4061–4065
6. Lazinski, D., Grzadzielska, E., and Das, A. (1989) Sequence-specific recognition of RNA hairpins by bacteriophage antiterminators requires a conserved arginine rich motif. *Cell* **59,** 207–218
7. Nodwell, J.R., and Greenblatt, J. (1993) Recognition of boxA antiterminator RNA by the *E. coli* antitermination factors NusB and ribosomal protein S10. *Cell* **72,** 261–268
8. Mogridge, J., Legault, P., Li, J., Van Oene, M. D., Kay, L. E., and Greenblatt, J. (1998) Independent ligand-induced folding of the RNA-binding domain and two functionally distinct antitermination regions in the phage λ N protein. *Mol. Cell* **1,** 265–275
9. Sen, R., Chalissery, J., and Muteeb, G. (2008) *Nus Factors of Escherichia coli, Module 4.5.3.1. EcoSal—Escherichia coli and Salmonella: Cellular and Molecular Biology* (Böck, A., Curtiss, R., III, Kaper, J. B., Karp, P. D., Neidhardt, F. C., Nyström, T., Slauch, J. M., and Squires, C. L., eds), American Society for Microbiology Press, Washington, D. C.
10. Yang, X., Molimau, S., Doherty, G. P., Johnston, E. B., Marles-Wright, J., Rothnagel, R., Hankamer, B., Lewis, R. J., Lewis, P. J. (2009) The structure of bacterial RNA polymerase in complex with the essential transcription elongation factor NusA. *EMBO Rep.* **10,** 997–1002
11. Ha, K. S., Toulokhonov, I., Vassylyev, D. G., and Landick, R. (2010) The NusA N-terminal domain is necessary and sufficient for enhancement of transcriptional pausing via interaction with the RNA exit channel of RNA Polymerase. *J. Mol. Biol.* **401,** 708–725
12. Mah, T. F., Kuznedelov, K., Mushegian, A., Severinov, K., and Greenblatt, J. (2000) The α subunit of *E. coli* RNA polymerase activates RNA binding by NusA. *Genes Dev.* **14,** 2664–2675
13. Schmidt, M. C., and Chamberlin, M. J. (1987) NusA protein of *Escherichia coli* is an efficient transcription termination factor for certain terminator sites. *J. Mol. Biol.* **195,** 809–818
14. Gusarov, I., and Nudler, E. (2001) Control of intrinsic transcription termination by N and NusA. The basic mechanisms. *Cell* **107,** 437–449
15. Farnham, P.J., Greenblatt, J., and Platt, T. (1982) Effects of NusA protein transcription termination in the tryptophan operon of *Escherichia coli*. *Cell* **29,** 945–951
16. Lau, L.F., Roberts, J.W., and Wu, R. (1983) RNA polymerase pausing and transcript release at the λ t_{R1} terminator *in vitro*. *J. Biol. Chem.* **258,** 9391–9397
17. Sigmund, C. D., and Morgan, E. A. (1988) Nus A protein affects transcrip-

tional pausing and termination *in vitro* by binding to different sites on the transcription complex. *Biochemistry,* **27,** 5622–5627
18. Mah, T. F., Li, J., Davidson, A. R., and Greenblatt, J. (1999) Functional importance of regions in *Escherichia coli* elongation factor NusA that interact with RNA polymerase, the bacteriophage λ N protein and RNA. *Mol. Microbiol.* **34,** 523–537
19. Muteeb, G., Dey, D., Mishra, S., and Sen, R. (2012) A multi-pronged strategy of an antiterminator protein to overcome Rho-dependent transcription termination. *Nucleic Acids Res.* **40,** 11213–11228
20. Muteeb, G., and Sen, R. (2010) Random mutagenesis using a mutator strain. *Methods Mol. Biol.* **634,** 411–419
21. Zheng, C., and Friedman, D. I. (1994) Reduced Rho-dependent transcription termination permits NusA-independent growth of *Escherichia coli*. *Proc. Natl. Acad. Sci. U.S.A.* **91,** 7543–7547
22. Chalissery, J., Banerjee, S., Bandey, I., and Sen, R. (2007) Transcription termination defective mutants of Rho. Role of different functions of Rho in releasing RNA from the elongation complex. *J. Mol. Biol.* **371,** 855–872
23. Cheeran, A., Babu Suganthan, R., Swapna, G., Bandey, I., Achary, M. S., Nagarajaram, H. A., and Sen, R. (2005) *Escherichia coli* RNA polymerase mutations located near the upstream edge of an RNA. DNA hybrid and the beginning of the RNA-exit channel are defective for transcription antitermination by the N protein from lambdoid phage H-19B. *J. Mol. Biol.* **352,** 28–43
24. Bonin, I., Mühlberger, R., Bourenkov, G. P., Huber, R., Bacher, A., Richter, G., and Wahl, M. C. (2004) Structural basis for the interaction of *Escherichia coli* NusA with protein N of phage λ. *Proc. Natl. Acad. Sci. U.S.A.* **101,** 13762–13767
25. Prasch S, Schwarz S, Eisenmann A, Wöhrl BM, Schweimer K, Rösch P. (2006) Interaction of the intrinsically unstructured phage λ N Protein with *Escherichia coli* NusA. *Biochemistry* **45,** 4542–4549
26. Van Gilst, M. R., and von Hippel, P. H. (1997) Assembly of the N-dependent antitermination complex of phage λ. NusA and RNA bind independently to different unfolded domains of the N protein. *J. Mol. Biol.* **274,** 160–173
27. Neely, M. N., and Friedman, D. I. (2000) N-mediated transcription antitermination in lambdoid phage H-19B is characterized by alternative NUT RNA structures and a reduced requirement for host factors. *Mol. Microbiol.* **38,** 1074–1085
28. Friedman, D. I., and Baron, L. S. (1974) Genetic characterization of a bacterial locus involved in the activity of the N function of phage λ. *Virology* **58,** 141–148
29. Zhou, Y., Mah, T. F., Yu, Y. T., Mogridge, J., Olson, E. R., Greenblatt, J., and Friedman, D. I. (2001) Interactions of an Arg-rich region of transcription elongation protein NusA with NUT RNA. Implications for the order of assembly of the λ N antitermination complex in vivo. *J. Mol. Biol.* **310,** 33–49
30. Zhou, Y., Mah, T. F., Greenblatt, J., and Friedman, D. I. (2002) Evidence that the KH RNA-binding domains influence the action of the *E. coli* NusA protein. *J. Mol. Biol.* **318,** 1175–1188
31. Beuth, B., Pennell, S., Arnvig, K. B., Martin, S. R., and Taylor, I. A. (2005) Structure of a *Mycobacterium tuberculosis* NusA-RNA complex. *EMBO J.* **24,** 3576–3587
32. Schweimer, K., Prasch, S., Sujatha, P. S., Bubunenko, M., Gottesman, M. E., and Rösch, P. (2011). NusA interaction with the α subunit of *E. coli* RNA polymerase is via the UP element site and releases autoinhibition. *Structure* **19,** 945–954
33. Cheeran, A., Kolli, N. R., and Sen, R. (2007) The site of action of the antiterminator protein N from the Lambdoid Phage H-19B. *J. Biol. Chem.* **282,** 30997–31007
34. Shankar, S., Hatoum, A., Roberts, J. (2007) A transcription antiterminator constructs a NusA-dependent shield to the emerging transcript. *Mol. Cell* **27,** 914–927
35. Sen, R., King, R. A., Mzhavia, N., Madsen, P. L., Weisberg, R. A. (2002) Sequence-specific interaction of nascent antiterminator RNA with the zinc-finger motif of *Escherichia coli* RNA polymerase. *Mol. Microbiol.* **46,** 215–222
36. Berdygulova, Z., Esyunina, D., Miropolskaya, N., Mukhamedyarov, D., Kuznedelov, K., Nickels, B. E., Severinov, K., Kulbachinskiy, A., and Minakhin, L. (2012) A novel phage-encoded transcription antiterminator acts by suppressing bacterial RNA polymerase pausing. *Nucleic Acids Res.* **40,** 4052–4063
37. Opalka N., Brown J., Lane W. J., Twist K. A., Landick, R., Asturias, F. J., Darst, S.A. (2010). Complete structural model of *Escherichia coli* RNA polymerase from a hybrid approach. *Plos Biol.* **8,** e1000483
38. Neely, M. N., and Friedman, D. I. (1998) Functional and genetic analysis of regulatory regions of coliphage H-19B. Location of shiga like toxin and lysis genes suggest a role for phage functions in toxin release. *Mol. Microbiol.* **28,** 1255–1267

The Interaction Surface of a Bacterial Transcription Elongation Factor Required for Complex Formation with an Antiterminator during Transcription Antitermination

Saurabh Mishra, Shalini Mohan, Sapna Godavarthi and Ranjan Sen

J. Biol. Chem. 2013, 288:28089-28103.
doi: 10.1074/jbc.M113.472209 originally published online August 2, 2013
